Cano-Pleite, E., Hernández-Jiménez, F., Garcia-Gutierrez, L. M. & Acosta-Iborra, A. (2017). Experimental study on the motion of solids around an isolated bubble rising in a vertically vibrated fluidized bed. *Chemical Engineering Journal*, vol. 330, pp. 120–133.

Experimental study on the motion of solids around an isolated bubble rising in a vertically vibrated fluidized bed

E. Cano-Pleite[a,*], F. Hernández-Jiménez[a], L.M. Garcia-Gutierrez[a], A. Acosta-Iborra[a]

[a]*Department of Thermal and Fluid Engineering, Carlos III University of Madrid, Av. de la Universidad 30, 28911, Leganés, Madrid, Spain*

Abstract

The motion of solids around isolated bubbles rising in a vertically vibrated pseudo-2D bed is experimentally studied in this work by combining Digital Image Analysis (DIA) and Particle Image Velocimetry (PIV). The bed material is Geldart B spherical particles. Different vibration amplitudes and frequencies are applied to the bed vessel while the bed is fluidized with air at minimum fludization conditions and isolated bubbles are sequentially injected in the bed. An averaging of bubbles method is presented and used to statistically characterize the average motion of solids around the bubbles. The results show that the presence of a bubble in the system perturbs the cyclic compression and expansion behavior of the bed bulk and, in particular, influences the velocity of the expansion wave front traveling upwards the bed. Analogously, the motion of solids around the bubble and, specially, in the bubble wake region, are strongly affected by the cyclic compression and expansion of the bed bulk. However, direct comparisons of the experimental results with the Davidson & Harrison potential flow model reveal that this model is still applicable for the prediction of the solids velocity around the bubble in a vertically vibrated fluidized bed.

Keywords: Fluidized bed, Vibration, Pseudo-2D, Bubble, PIV

1. Introduction

Vibration of a gas fluidized bed tends to break gas channeling and agglomeration, facilitate fluidization and enhance mixing or segregation depending on the vibration strength and the superficial gas velocity. Vibration is also a way of stabilizing the system and gain some control on the bed dynamics [1–5]. Despite its advantages, vibration introduces complexities in the dynamics of the bed that are far from being fully understood. Knowledge of these complex physical phenomena arising from vibration of a fluidized bed may be used to improve design and control of the existing Vibrated Fluidized Beds (VFBs) and to increase their range of operation to new applications.

---

*Corresponding author. Tel:+34 91 624 8884
Email address: edcanop@ing.uc3m.es (E. Cano-Pleite)

Among the different experimental techniques aimed at characterizing the bed and bubble behaviors in VFBs, Digital Image Analysis (DIA) is one of the most used, not only in VFBs but also in conventional fluidized beds [5–17]. In general, this technique makes use of pseudo two-dimensional (pseudo-2D) beds (i.e. beds of small thickness), which posses a transparent wall to allow optical access to the interior of the system. This also allows the use of Particle Image Velocimetry (PIV) techniques, which have been also extensively used in the characterization of the particle movement in conventional fluidized beds [11, 12, 18–21]. This technique can be useful to validate existing models of the solids motion inside conventional (non-vibrated) fluidized beds as, for example, the potential flow theory developed in the early 1960s by Davidson and Harrison [22]. In this regard, Müller et al. [18] studied the eruption of a bubble in a fluidized bed by means of PIV. They observed that, even after eruption, the potential flow theory was capable of predicting the velocity of the particles on the roof of the bubble. Hernández-Jiménez et al. [23] carried out two-fluid model simulations of the system used in [18]. The results of the simulations indicated that the potential flow theory provides a more accurate prediction for the particle velocities in erupting bubbles than other semi-empirical relations available in the literature. However, the use of PIV in vibrated fluidized beds is still very reduced [15, 24, 25].

Existing experimental and computational studies in VFBs are mainly focused on beds operated in bubbling regime. These works include studies on the effect that vibration has on the bed and bubble dynamics [1, 5], the air pressure and void fraction fluctuations induced by vibration [26–28] and the aggregation [28] and segregation phenomena [3, 16, 29–31]. Some works have also investigated the effect of vibration on the bubble behavior in VFBs [6, 8, 9]. A change of the flow pattern in the vibrated bed with regard to a conventional bed was observed by Mawatari et al. [7] and Cano-Pleite et al. [10]. Cano-Pleite et al. [14] studied the oscillatory behavior of the bed bulk and bubbles. The results in [10, 14] show that both the mean and oscillatory behavior of bubbles is different in the upper and lower sections of a freely bubbling bed. The change of behavior of the bubbles depending on their vertical coordinate in the bed was also observed in experiments and Two-Fluid Model simulations devoted to isolated bubbles rising in a fluidized bed at minimum fluidization conditions [32, 33]. However, there is a lack of characterization of the motion of solids around bubbles in vibrated fluidized beds. Knowledge of this motion of solids can further clarify the interaction of bubbles with the bed bulk and contribute to the validation of simulation models.

The aim of the present work is to experimentally study the motion of particles in the bed bulk and the vicinity of an isolated bubble rising in a vibrated fluidized bed. These novel results are presented using a bubble averaging method, which averages the bubble contours and the velocity of solids in the proximity of the bubbles. The bubble averaging method is used to determine for the first time the validity of the Davidson and Harrison [22] model for the particle motion around a bubble rising in a vibrated fluidized bed. Comparison of the motion of solids around an isolated bubble with Davidson and Harrison [22] potential flow model can be useful for clarifying the essential mechanisms affecting the oscillatory motion of bubbles

in a vibrated bed and the effect of the compression-expansion waves traveling inside the bed bulk. The PIV analysis here presented constitutes a necessary step in the understanding of the behavior of bubbles in freely bubbling beds subjected to vibration. This may affect, for example, the volume of solids dragged by the bubble, which in turn has a deep impact on the fuel motion and the mixing characteristics in reactors and fluidized bed processes.

2. Experimental setup

Figure 1 shows a sketch of the experimental facility used in the present work. The bed vessel consists in a pseudo-2D fluidized bed of dimensions 0.3 x 0.6 x 0.01 m (width W, height H and thickness K, respectively). The bed was placed on a vibrating structure. The front and rear walls of the bed were made out of glass and the rear wall was painted in black to increase contrast of the dense and bubble phases. The bed vessel was filled with ballotini glass beads with a size range between 425 and 600 μm and a density of 2500 kg/m^3 (Geldart's classification type B [34]). Approximately a 5% of the particles were painted in black to enhance the cross-correlation of the bed images during their processing by Particle Image Velocimetry (PIV). The minimum fluidization velocity of the particles at static conditions was measured using the mean value of the signal of a pressure probe attached to the rear wall of the bed at 0.025 m above the distributor and resulted in $U_{mf} = 0.28$ m/s.

[Figure 1 about here.]

Vibration was induced to the bed by means of two vibro-motors (Italvibras MVSI 10/310 SO2) symmetrically placed on the vibrated structure at each side of the bed. The vibro-motors produced a vertical sinusoidal displacement of the bed vessel, $\delta(t) = A\sin(2\pi f t)$. The amplitude of vibration, A, was varied by changing the relative position of the two pair of eccentric masses inside each of the vibro-motors. The frequency of vibration, f, was controlled by changing the turning velocity of the motors. Due to the characteristics of the vibro-motors, slight changes in the vibration amplitude were observed when varying the vibration frequency (see Table 1). More details about the experimental facility can be found in [32, 35].

Similarly to [32], two independent air supply lines were employed for the fluidization of the bed and the injection of bubbles in the system. An air supply line was used to reach minimum fluidization conditions in the bed. A secondary air supply was used to inject isolated bubbles in the bed through a hole drilled through the rear wall of the vessel at 5 cm above the distributor. In order to obtain bubbles of approximately the same size, a gas volume was preloaded between two valves (see 'Valve 1' and 'Valve 2' in Figure 1). In consequence, the mass of air injected could be controlled by varying the volume and pressure of the gas between the two valves. To avoid the influence of the bed lateral walls on the motion of solids in the bubble vicinity, bubbles smaller than one third of the width of the bed are injected in the bed.

A high speed camera (Redlake Motion pro X3) was employed to record images of the front view of the bed at a frame rate of 250 images per second. Two spotlights were symmetrically placed at both sides of the bed to uniformly illuminate its front view and to enhance the contrast between the dense and bubble phases of the images. To obtain the bed instantaneous displacement, $\delta(t)$, and similarly to previous works [15, 32], five white squares of small size were glued to the plenum as a reference, as shown in Figure 1. The vertical instantaneous position of the bed was obtained from the centroid location of these reference squares. The frequency of vibration of the bed vessel, f, was measured by performing a frequency domain analysis (Welch periodogram) of the instantaneous position of the squares. Once the bed instantaneous displacement is calculated for every image, the equivalent vibration amplitude and velocity of the bed were determined with:

$$A = \sigma_{\delta(t)}\sqrt{2} \tag{1}$$

$$V_{bed} = \sigma_{v(t)}\sqrt{2} \tag{2}$$

where $v(t) = d\delta(t)/dt$ is the instantaneous vertical velocity of the bed vessel, $\sigma_{\delta(t)}$ and $\sigma_{v(t)}$ are, respectively, the standard deviation of the time evolution of $\delta(t)$ or $v(t)$ with regard to their mean.

Each of the conducted experiments comprised a recording time of around 14 seconds, which corresponded to the injection of, approximately, 10 isolated bubbles along an experiment. The images started to be acquired around 10 seconds after turning on the vibro-motors to avoid the recording of start-up effects. Once the bed started to be recorded, bubbles were sequentially injected in the bed.

The different experiments carried out in the present work are listed in Table 1. Experiment 1 was the central case with $A = 4.2$ mm and $f = 14.2$ Hz. The effect of the vibration frequency and amplitude were investigated by independently increasing f and increasing or decreasing A around the values chosen for Experiment 1. In all the experiments, the static bed height was $H_0 = 0.375$ m ($H_0/W = 1.25$). H_0 was considered large enough to characterize the motion of isolated bubbles along the bed height. It was observed that larger static bed heights (e.g. $H_0/W = 1.5$) increased the particle rain inside the bubbles, which complicated the determination of the solids velocity on top of the injected bubbles.

[Table 1 about here.]

3. Theory

3.1. Potential flow description of the solids velocity around a bubble

The solids velocities obtained from the experiments are compared with those resulting from the potential flow model around a bubble proposed by Davidson and Harrison [22]. Figure 2 shows a schematic drawing of the solids motion around a bubble rising in a non-vibrated fluidized bed.

4

[Figure 2 about here.]

Davidson and Harrison [22] used the potential flow theory around a cylinder or a sphere to predict the motion of particles around a bubble in a conventional fluidized bed. The velocity potential, Φ, is governed by the Laplace equation:

$$\nabla^2 \Phi = 0 \tag{3}$$

As a first approximation, the bubble and the portion of its solidary wake is assumed to be cylindrical in a two-dimensional bed. The solids velocities in the horizontal, x, and vertical, y, directions are calculated with:

$$u = \frac{\partial \Phi}{\partial x} \tag{4}$$

$$v = \frac{\partial \Phi}{\partial y} \tag{5}$$

where x and y are the horizontal and vertical coordinates with origin at the center of the circle that defines the bubble contour. In Equations (4) and (5) u and v are the solids velocities in a system of reference attached to the bubble center ($x = 0$, $y = 0$). The velocity potential around a rising bubble in a 2D fluidized bed was defined by Davidson and Harrison [22] as:

$$\Phi_{xy} = -V_{bub} \left(\frac{R_b^2}{x^2 + y^2} \right) (y \cos(\theta_b) + x \sin(\theta_b)) \tag{6}$$

where R_b is the bubble radius, V_{bub} is the bubble velocity and θ_b is the rising angle of the bubble with respect to the vertical direction.

Following Hernández-Jiménez et al. [12], the solids velocity in the horizontal and vertical directions can be expressed in cartesian coordinates as a function of the distance to the bubble centroid:

$$u(x, y) = \left(\frac{V_{bub} R_b^2}{x^2 + y^2} \right) \left(\frac{2x(y \cos(\theta_b) + x \sin(\theta_b))}{x^2 + y^2} - \sin(\theta_b) \right) \tag{7}$$

$$v(x, y) = \left(\frac{V_{bub} R_b^2}{x^2 + y^2} \right) \left(\frac{2y(y \cos(\theta_b) + x \sin(\theta_b))}{x^2 + y^2} - \cos(\theta_b) \right) \tag{8}$$

If a bubble rises in the bed in the vertical direction (i.e. $\theta_b = 0$), the solids velocity described through Equations (7) and (8) can be simplified to yield:

$$u(x, y) = 2V_{bub} xy \left(\frac{R_b}{x^2 + y^2} \right)^2 \tag{9}$$

5

$$v(x, y) = V_{bub}(y^2 - x^2) \left(\frac{R_b}{x^2 + y^2} \right)^2 \qquad (10)$$

4. Data processing

4.1. Bubble detection

The software Matlab® was employed for the processing of the images recorded with the high speed camera and to calculate the bubble properties and the velocity of the particles in the bed. Firstly, the bubbles present in the system were detected using DIA by applying a constant threshold value [36] to the images of the front view of the bed. With this threshold, each pixel in the original image was assigned to a new value: 0 if the pixel corresponded to a bubble and 1 if it corresponded to the dense phase. A previous work devoted to the oscillation of the bubble diameter and velocity of bubbles rising in a vibrated fluidized bed has demonstrated that the particle rain may cyclically affect the bubble diameter oscillation depending on the bubble position along the bed height [14]. Therefore, to reduce the effect of the particle rain on top of the bubble and the possible fictitious bubble splitting due to this effect, the threshold was combined with a circular erosion and dilation of the bubble contour extended 4 pixels in the radial direction. Secondly, the bubble equivalent diameter, D_b, was calculated as the diameter of a circle having the same area as the bubble, A_b.

$$D_b = \sqrt{\frac{4A_b}{\pi}} \qquad (11)$$

The instantaneous vertical velocity of a bubble, $V_b(t)$, was obtained with the vertical displacement of the bubble centroid between two consecutively recorded images divided by the time increment, Δt between these two images. Note that the bubble and solids velocities can be calculated in an absolute (the high speed camera) or a relative (the distributor) system of reference. In the present work, both the instantaneous bubble vertical velocity $V_b(t)$ and the solids velocity (see Section 4.2) were computed in an absolute system of reference.

$$V_b(t) = \frac{y_b(t + \Delta t) - y_b(t)}{\Delta t} \qquad (12)$$

4.2. Particle Image Velocimetry

The solids velocity, $\vec{v}_s$, in the bed bulk was calculated by means of PIV. Previously, for each image, a mask that discriminates between the dense phase and the bubble phase is used. This mask is developed by means of DIA and allows the calculation of the velocity vectors exclusively in the regions identified as dense phase during the bubble detection procedure. The code MATPIV 1.6.1. [37] was used for the calculation of the solids velocity. The MATPIV code possesses multigrid processing and a final interrogation window

size of 16x16 pixels with 50% overlapping was selected. A signal-to-noise ratio equal to 1.3 [38], a global histogram operator with an acceptance region with factor 4, a median local filter and an interpolation of the outlier vectors were also applied during the processing of the vector field.

The velocity of solids around a bubble was also investigated in this work as a function of the phase of the bed vessel by means of an averaging of cycles method [14, 15, 32, 33]. As the bed manifests a cyclic behavior of period T, the cyclic oscillation of the bed vessel in each period can be divided into M phase intervals $\left(\dfrac{2(k-1)\pi}{M} < \phi < \dfrac{2k\pi}{M} \right)$ $k = 1...M$, to describe the transient behavior of the particles in terms of the phase, $\phi \in [0, 2\pi]$ instead of the time. $M = 8$ was chosen in this work. With this value of M, the resulting phase intervals are considered sufficiently small to allow a resolved characterization of the bubble behavior as a function of the vibration phase and large enough to provide statistically meaningful results in each of the phase intervals. Hence, the time average velocity of the solids at every phase interval can be calculated with the following conditional mean:

$$\vec{v}_{s,\phi_k}(x,y) = \frac{\sum_{i=1}^{N} \vec{v}_{s,i}(x,y)\delta_{i,k}}{\sum_{i=1}^{N} \delta_{i,k}} \tag{13}$$

where $\vec{v}_s$ is the solids velocity vector in the ith frame, N is the number of total frames along an experiment and $\delta_{i,k}$ is equal to the unity if the phase ϕ_i of the ith frame is within the kth interval of phase.

$$\delta_{i,k} = \begin{cases} 1 & \text{if } \frac{2(k-1)}{M}\pi < \phi_i < \frac{2k}{M}\pi \\ 0 & \text{otherwise} \end{cases} \tag{14}$$

Here, the phase $\phi_i = 0$ (beginning of each cycle) corresponds to the bed vessel at its central position and moving upwards at an instant t_0 and $\phi_i = 2\pi$ (end of the cycle) to the bed vessel again at its central position and moving upwards at a time instant $t_0 + T$.

4.2.1. Bubble averaging method

To statistically characterize the particle velocity around bubbles, the present work proposes a method to average the bubble contours on an equivalent bubble whose behavior is representative of all the bubbles along a whole experiment or in a specific phase range. This method allows to directly compare the experimental solids motion around the equivalent bubble with those from the Davidson and Harrison [22] potential flow model, i.e. the vibration-free model for an isolated bubble described in Section 3. The bubble averaging method consists in averaging all the bubbles identified along an experiment in order to obtain the average distribution of the solids velocity around a representative bubble that statistically represents all the analyzed bubbles. The bubble averaging method is described in the following lines and schematized in Figure 3.

[Figure 3 about here.]

For every image frame (numbered with i) in which an isolated bubble is present in the system, the instantaneous area-equivalent bubble diameter ($D_{b,i}$), velocity ($V_{bub,i}$), the coordinates describing its centroid, ($(x,y)_{b,i}^{(C)}$) and its perimeter ($(x,y)_{b,i}^{(P)}$) are obtained by means of DIA. The contour of the bubble is normalized and translated to a new system of coordinates defined by a normalized pair of coordinates (X,Y). In this new coordinate system, the bubble centroid is assigned to the origin, $X = 0$ and $Y = 0$, and the bubble contour is normalized with the radius of the bubble. By this, all the bubbles' centroids are placed at $X = 0$ and $Y = 0$ with a radius equal to unity. Thus, the normalized bubble contour in the new coordinate system is:

$$(X,Y)_{b,i}^{(P)} = \frac{2[(x,y)_{b,i}^{(P)} - (x,y)_{b,i}^{(C)}]}{D_{b,i}} \tag{15}$$

This operation is repeated for all the bubble contours identified along an experiment, which comprises several bubbles injected one after the other. The average contour $(X,Y)_{b,avg}^{(P)}$ is defined as the contour that averages all the analyzed bubbles, as schematized in Figure 3(b):

$$(X,Y)_{b,avg}^{(P)} = \frac{\sum_{i=1}^{N_b}(X,Y)_{b,i}^{(P)}\beta_{i,k}}{\sum_{i=1}^{N_b}\beta_{i,k}} \tag{16}$$

where N_b is the number of analyzed bubble contours and $\beta_{i,k}$ is equal to the unity if the ith bubble centroid is within a specific distance from the distributor, $y_{b,i} \in [y_{b,min}, y_{b,max}]$ and the phase of the bed vessel is within the kth phase interval of the period of oscillation:

$$\beta_{i,k} = \begin{cases} 1 & \text{if } \left(\frac{2(k-1)}{M}\pi < \phi_i < \frac{2k}{M}\pi\right) \text{ and } (y_{b,min} < y_{b,i} < y_{b,max}) \\ 0 & \text{otherwise} \end{cases} \tag{17}$$

The same operation is carried out for the solids velocity vectors, $\vec{v}_s(x,y)_i$, around the bubble. In this case, normalization is carried out dividing by the mean velocity of the centroid of all the analyzed bubbles. Thus, the value of the normalized solids velocity in the new coordinate system for each of the bubbles is calculated as:

$$\vec{V}_s(X,Y)_i = \frac{\vec{v}_s(x - x_{b,i}^{(C)}, y - y_{b,i}^{(C)})_i}{\frac{1}{N_b}\sum_{i=1}^{N_b}V_b} \tag{18}$$

Note that the position of the velocity vectors, $\vec{V}_s(X,Y)_i$ for each of the frames in the new system of coordinates (X,Y) may vary from one frame to another, since they are displaced during the normalization of x and y. Thus, the average solids velocity around the bubble is obtained by dividing the new system of coordinates in N_{bins} interpolating windows. These windows have approximately the same size as the normalized distance between PIV vectors in the initial PIV image. The normalized solids velocity vectors of each bubble $\vec{V}_s(X,Y)_i$ are linearly interpolated to the center of each of the interpolating windows, obtaining

8

the average of normalized velocity $\vec{V}_s(X,Y)_{avg}$ of solids around the averaged bubble contour, $(X,Y)_{b,avg}^{(P)}$, as shown in Figure 3(b).

Once all the bubble contours and the velocity vectors are averaged in the new coordinate system, the normalized mean solids velocity of the particles as a function of the angle around a bubble, θ, could be determined (see Figure 3(c)). Here, θ is the angle between the position of the velocity vector and a vertical line passing through the bubble centroid. In order to do this, firstly the coordinates of the circle, $(X,Y)^{(F)}$ that better fits the average bubble contour $(X,Y)_{b,avg}^{(P)}$ in an angle range $\theta \in [-120°, 120°]$ (i.e. the circle with radius R in Figure 3 skipping the bubble wake) are calculated. Secondly, to avoid the effect of particle rain on the calculation of the solids motion around the bubble, a new fitting circle, $(X,Y)_n^{(F)}$ is used. This new circle is obtained by increasing the radius of the fitting circle $(X,Y)^{(F)}$ to a radius R^* at which the velocity of the particles at the vertical line, $\theta = 0°$, reaches a maximum positive value (see Figure 3(c)). Here, $\theta = 0°$ because the horizontal component of the bubble velocity of each bubble is very reduced compared to the vertical component. This radius R^* defines the minimum distance to the bubble centroid for which the experimental solids velocity presents a decrease with an increase of the radius, as predicted by the potential flow theory. Results for distances to the bubbles smaller than R^* do not show this decrease of $\vec{V}_s(X,Y)_{avg}$ and, hence, are considered severely affected by the particle rain inside the bubble and the irregularities of the bubble contour.

As schematized in Figure 3(c), the average solids velocity as a function of θ was obtained by interpolating the average of normalized solids velocity vectors $\vec{V}_s(X,Y)_{avg}$ to the contour of the new circle $(X,Y)_n^{(F)}$.

5. Results and discussion

The results presented in this work are divided into two main sections. In the first section, the interaction of the bubbles with the oscillating velocity of the bed bulk in a vertically vibrated fluidized bed is examined. These results serve as a basis to understand the effect of vibration on the solids motion around the bubble, which is also compared with the Davidson and Harrison [22] classical potential flow model in the second results section.

5.1. Bulk behavior

Previous works devoted to vibrated fluidized beds operated at minimum fluidization conditions have shown a cyclic compression and expansion of the bed bulk. This cyclic behavior of the bed bulk creates compression and expansion waves that travel through the bed [10, 14, 15, 32, 33] regardless of the size of the particles employed. The presence of the bubble in the system may change the motion of the surrounding bed bulk and vice versa. Thus, a characterization of the motion of the particles in the bed bulk with bubbles is a necessary step before attempting to study the motion of solids around the bubble.

To analyze the bed bulk motion and the behavior of the solids velocity waves in the bed, Figure 4 compares the phase evolution of the absolute vertical velocity of solids along the vertical direction with and without a bubble rising in the bed. This phase evolution was obtained by using the averaging of cycles method on the solids velocity, which was calculated by means of PIV (see Section 4.2). The solids velocity was sampled in two vertical stripes of width of $\Delta x \simeq 0.02$ m (three PIV windows) symmetrically placed at an approximate distance of $x_s = W/8$ from the bed left and right walls. This position of the vertical stripes was chosen so that the volume of the injected bubbles did not cross the vertical stripes. When no bubble was present in the system, the solids velocity was also sampled in a vertical stripe of the same width situated in the central section of the bed (i.e. $x_s = W/2$). In Figure 4, every curve represents the average profile of the solids vertical velocity in the two lateral stripes along the whole bed height. In the figure, the solids vertical velocity was normalized with the bed vessel velocity, V_{bed}. Results are separated in $M = 16$ consecutive phase intervals of $\Delta \phi = 2\pi/M$. The standard deviation of the instantaneous velocity, with regard to the averaged values within each phase and height intervals presented in Figure 4, can be calculated to quantify the uncertainty of the results. Thus, for $\Delta \phi = \pi/8$ rad and every height interval, the resulting standard deviation of V/V_{bed} is in the range of 0.06-0.15 in Figure 4(a), 0.05-0.18 in Figure 4(b) and 0.06-0.17 in Figure 4(c). This indicates that the uncertainty of the PIV profiles in Figure 4 is relatively low.

[Figure 4 about here.]

In Figure 4(a) no bubbles are present in the system and, hence, the bed bulk cyclically expands and compresses without being perturbed by bubbles. For $\phi = 3\pi/2$ rad, the bed vessel commences to move upwards and impacts the bed bulk, which creates a compression wave of solids that travels upwards in the bed bulk. As in [15], the compression wave front divides the bed into two regions with different relative velocities: upward velocity below the wave front and downward velocity above the wave front. Similarly, when the bed vessel starts to move downwards at $\phi = \pi/2$ rad, an expansion wave traveling upwards the bed appears. The expansion wave front also separates the bed in two regions of solids velocity moving downwards below the wave front and upwards above the wave front. In general, the front of the expansion wave is less pronounced and produces a softer change in the velocity of solids than the front of the compression wave.

Figure 4(b,c), shows the average solids velocity in the vertical stripes when a bubble is situated at $y_b = 0.1 - 0.2$ m (Figure 4(b)) and $y_b = 0.2 - 0.3$ m (Figure 4(c)) from the distributor. Note that these figures are the result of the averaging of cycles of the isolated bubbles sequentially injected in the experiment and therefore the injection of bubbles was produced at random phases in the vibration cycle. In Figure 4(b,c), the motion of the solids belonging to the bed bulk is modified when a bubble is present in the system. During the compression stage of the bed bulk, the opposite velocities of the bed bulk regions (i.e. positive velocity of solids in the lower section of the bed and negative in the upper section of the bed) also appear. However, contrary to the case without bubble in Figure 4(a), the maximum negative velocity of particles during the

expansion stage of the bed bulk (i.e. $\phi = \pi - 2\pi$ rad) takes place at the average bubble height ($y \simeq 0.15$ m in Figure 4(b) and $y \simeq 0.25$ m in Figure 4(c)). This can be explained as follows. The presence of the bubble reduces the section volume through which the bulk of particles descends at the lateral sides of the bubble. This may promote a larger downward velocity of particles at the vicinity of the bubble and the reduction of the upwards solids velocity in the region above the bubble. Both effects lead to the commented minimum velocity of particles.

The position and velocity of the compression and expansion wave fronts were calculated using the vertical coordinate, in the vertical stripe, at the point at which the absolute vertical velocity of the particles is equal to half the maximum absolute value of the vertical velocity of solids in the vertical stripe. As the bed bulk impacts the bed vessel in a phase $\phi \simeq 3\pi/2$ rad, the compression wave position is calculated in an interval starting at $\phi = 3\pi/2$ rad and ending at $\phi = 7\pi/2$ rad (i.e. $\phi = \pi/2$ rad of the next cycle), which corresponds to the ascending stroke of the bed vessel. Equivalently, the expansion wave position is calculated in a phase interval $\phi = \pi/2 - 3\pi/2$ rad.

Figure 5(a) shows the position of the compression and expansion wave fronts as a function of the vibration phase and for the lateral ($x_s = W/8$) and central ($x_s = W/2$) vertical stripes when no bubbles were present in the system. The positions of the compression and expansion wave fronts close to the lateral walls of the bed are higher than those in the central stripe for the same phase. This is due to the presence of the lateral walls, as in [15]. This makes that the particles close to the corners of the bed impact the base of the bed earlier than the particles on the distributor center and they can easily follow the upward motion of the distributor, which slightly increases the propagation velocity of the wave front. This same phenomena is observed for the expansion wave in Figure 5(a).

[Figure 5 about here.]

In Figure 5(b), the positions of the compression and expansion wave fronts are modified when a bubble is present in the bed. Here, the wave fronts were calculated at $x_s = W/8$. Note that the wave front position at $x_s = W/2$ when bubbles are injected cannot be calculated because the presence of the bubble perturbs the solids velocity along the vertical stripe. As commented in Section 2, to reduce the effect of the lateral walls on the motion of solids around the bubble, the diameter of the injected bubbles was always smaller than one third the width of the vessel. In the case the bubbles were larger, the presence of the lateral walls of the bed vessel would promote an increase of the vertical descending velocity of the solids on the sides of the bubble. This would lead to values of the velocity profiles around the average bubble that may largely differ from those predicted by the Davidson and Harrison [22] potential flow model.

The propagation velocity of both the compression and expansion wave fronts can be calculated as:

$$V_{prop} = 2\pi f \frac{\Delta y_f}{\Delta \phi} \tag{19}$$

11

where y_f is the vertical position of the wave front shown in Figure 5 and $\Delta\phi$ is the phase variation between two consecutive positions of the wave fronts separated Δy_f apart.

When a bubble is located close to the distributor, $y_b = 0.1 - 0.15$ m, both the compression and the expansion wave fronts are closer to the distributor than when the bubble is higher (e.g. $y_b = 0.25 - 0.3$ m) for the same vibration phase (see Figure 5). This suggests that the bed bulk impacts the distributor progressively earlier in phase as the bubble rises in the bed. When the compression wave is originated, it travels upwards in the bed at a similar velocity regardless of the bubble vertical position ($V_{prop,c,avg} = 10.8$ m/s). When no bubble is present in the system, the average velocity of the compression wave is greater in the lateral section of the bed, $V_{prop,c,avg} = 14$ m/s at $x_s = W/8$, than at the center of the bed, $V_{prop,c,avg} = 9.4$ m/s at $x_s = W/2$.

The sound propagation velocity in a fluidized bed can be calculated following [39] as:

$$u_s = u_{s0}\sqrt{\frac{\rho_g}{\gamma\varepsilon[\rho_p(1-\varepsilon) + \rho_g\varepsilon]}} \tag{20}$$

where u_{s0} is the velocity of sound in the gas, ρ_g and ρ_p are the density of the gas and the particles, ε is the bed voidage and γ is the heat capacity ratio of the air. For the experimental conditions of this work, Equation (20) yields an effective velocity of sound of around 13 m/s, which is in accordance with the values of $V_{prop,c,avg}$ obtained before. This confirms that the compressibility of the gas phase plays a key role on the upwards propagation of the compression wave in the bed regardless the existence of a bubble in the system, as was suggested in [14, 15, 32, 33]. A more detailed study of the propagation of the compression wave in a bed operated at minimum fluidization conditions, together with a visualization of the compression and the expansion waves traveling through the bed bulk, can be found in [15]. In the case no bubble is present in the system, the expansion wave propagates at a velocity smaller than the compression wave ($V_{prop,e,avg} = 6.2$ m/s at $x_s = W/8$ and $V_{prop,e,avg} = 6.3$ m/s at $x_s = W/2$). However, as seen in Figure 4, the behavior of the expansion wave is largely affected by the presence of the bubble. In this case, the velocity of the expansion wave progressively increases from values of $V_{prop,e} = 1$ m/s when the bubble is situated in the $y_b = 0.1 - 0.15$ m interval to $V_{prop,e} = 9.5$ m/s when the bubble is present in a higher vertical coordinate in the bed ($y_b = 0.25 - 0.3$ m).

5.2. Isolated bubble behavior

It was evidenced in the previous section that the presence of the bubble in the system changes the motion of solids in regions far from the bubble as well as the behavior of the compression and expansion waves of solids traveling through the bed bulk. Thus, the motion of solids just around the bubble is presumably affected by these compression and expansion waves.

Figure 6 shows an example of four consecutive snapshots of a bubble rising in the vibrated fluidized bed. The snapshots belong to different instants within the same oscillation period of the bed vessel oscillation, as

indicated at the top of the figure. Figure 6(b) shows the instantaneous vectors of the absolute solids velocity superimposed to each of the snapshots. Note that the absolute system of coordinates (x, y) in Figure 6(a) is referred to the bottom left corner of the bed and has been changed in Figure 6(b) to a new system of coordinates (X, Y) when computing the solids velocity vectors, so that the bubble is centered at the origin of the new system, as indicated in Section 4.2.1.

Figure 6(b) also indicates the volume of particles dragged by the bubble wake, which has been arbitrarily defined in the figure as the volume below the bubble center (i.e. $Y < 0$) comprising the particles with upwards relative solids velocity. It can be observed that the volume of particles dragged by the bubble is larger in the first and last snapshots of Figure 6(b), revealing that the bubble wake is directly affected by the presence of the compression and expansion waves traveling upwards the bed.

In the second and third snapshots shown in Figure 6(b) the bed vessel descends and the bed bulk expands, according to Figure 4. During the descending stroke of the bed vessel, the bubble velocity decreases and, also, a negative relative velocity of the solids of the bed bulk at the right and left sides of the bubble appears due to the expansion of the bed bulk. However, the particles immediately below the bubble contour are not affected by this downward solids velocity and maintain their inertial upward displacement. This causes the partial penetration of the bubble wake in the interior of the bubble contour, producing the characteristic wavy contour of bubbles in a vibrated fluidized bed, which was also observed in previous works [10, 32].

The bed vessel impacts the bed bulk in a phase close to $\phi = 1.5\pi$ rad. This promotes an upward velocity of particles below the bubble, as reflected in the fourth snapshot of Figure 6(b). The volume of particles that penetrate the bubble decreases from the first to the second snapshot of Figure 6(b) due to the increase of the bubble velocity and the collapse of the particles that penetrated the bubble in previous phases of the cycle.

Despite the present work considers a single particle size, both the wavy contour at the bottom region of the bubbles and the cyclic compression and expansion of the bed bulk appear in beds of particles of different size [10, 14, 15, 32, 33]. Also, in [14], the oscillatory motion of the bubbles, which is mainly affected by the bed bulk cyclic compression and expansion, was qualitatively similar for different particle and bubble sizes even if the vibrated bed was operated in fully bubbling regime. This suggests that the behavior of the particles around the bubbles is qualitatively the same for other particle diameters and bubble sizes different to those analyzed here.

[Figure 6 about here.]

It can be observed in Figure 6(b) that, regardless of the vibration phase of the bed vessel, there is a region around the bubble in which the solids motion is strongly influenced by the presence of the bubble. The solids present an upward absolute velocity on top of the bubble, as the bed particles are pushed upwards due to the bubble ascending motion. The solids move around the bubble following the bubble contour, as in

13

an isolated bubble rising in a conventional fluidized bed without vibration [18, 22, 23]. Also, in the figure, between $\phi = 0.7\pi$ rad and $\phi = 1.4\pi$ rad ($\phi = 2.22 - 4.35$ rad), the contour of the bubble close to its wake is deformed because part of the wake penetrates into the bubble changing the shape of the bubble. This wavy shaped contour is characteristic of vibrated fluidized beds [10, 32, 33].

Figure 7 represents the streamlines and the module of the normalized absolute solids velocity around the average contour of bubbles rising in the vibrated fluidized bed and located within the vertical interval $y_b = 0.1 - 0.3$ m. To characterize the solids motion as a function of the oscillatory displacement of the bed vessel, the solids velocities are averaged within phase intervals of size $\Delta\phi = 0.25\pi$ rad. As can be seen in Figure 7, the solids motion close to the bubble contour and in the surroundings of the bubble varies significantly with the vibration phase.

In the phase interval $\phi = 0 - 0.25\pi$ rad of Figure 7(a), there exists a high ascending velocity of particles below the bubble contour, which is caused by the front of the compression wave of solids that is generated at the bottom of the bed. However, the presence of the bubble in the system perturbs this ascending motion of solids, as they are dragged upwards by the bubble wake. This behavior is also observed in the phase interval $\phi = 0.25\pi - 0.5\pi$ rad (Figure 7(c)). Nonetheless, when the bed vessel commences to descend in the phase interval $\phi = 0.5\pi - 0.75\pi$ rad (Figure 7(c)) the velocity of the solids below the bubble decreases significantly, as solids begin to move downwards following the bed vessel oscillatory motion. The expansion of the bed bulk commences in this phase interval, as manifested in Section 5.1, and a region of low solids velocity appears in the vicinity of the bubble. However, the region of particles that are in direct contact with the bubble contour are strongly affected by the presence of the bubble and move around it following its contour. This happens regardless the vibration phase and the behavior of the bed bulk around the bubble. During the subsequent phase intervals (i.e. $\phi = 0.75\pi - 1.5\pi$ rad in Figure 7(d-f)) the solids present a descending absolute velocity produced by the descending motion of the bed bulk, which causes the formation of a solids expansion wave front that travels upwards in the bed. This promotes a descending flow of solids in the whole bed except in the regions directly affected by the presence of the bubble. The bed bulk impacts again the distributor in a phase close to $\phi = 1.5\pi$ rad and the behavior described in the above lines is cyclically repeated.

[Figure 7 about here.]

To obtain the solids motion relative to the bubble displacement in the bed, Figure 8 illustrates the solid streamlines and velocity magnitude around an isolated bubble in a system of coordinates that moves at the same vertical velocity as the bubble front, which is defined as the vertical velocity of the solids at the fitting circle $(X, Y)_n^{(F)}$ (see Section 4.2.1) and within an angle $\theta \in [-10°, 10°]$. Here θ is the angle between a given point and the vertical line passing through the bubble center, as shown in Figure 3. Thus, for each normalized solids velocity vector average value $\vec{V}_s(X, Y)_{avg}$, in Figure 7, a new normalized relative velocity

14

of solids is computed following (21):

$$\vec{V}_r(X,Y) = \vec{V}_s(X,Y)_{avg} - \int_{\theta_i=-10°}^{\theta_f=10°} \frac{\vec{V}_{s,avg}(R(\theta)_n)d\theta}{\theta_f - \theta_i} \tag{21}$$

For all the phase intervals shown in Figure 8, the motion of solids around the average bubble resembles that of a potential flow around a bubble in a conventional fluidized bed (Equations (4) and (5), Davidson and Harrison [22]). Nevertheless, the solids behavior around the bubble is partially modified by the cyclic expansion and compression of the bed bulk. This is specially noticeable in the region below the bubble, in which the bubble is affected by the interaction of the bubble wake with both the compression and the expansion wave fronts of solids traveling in the bed.

[Figure 8 about here.]

In order to quantitatively characterize the velocity of particles around the bubble as a function of the vibration phase of the bed, a direct comparison between the solids velocity and the potential flow model is carried out in Figure 9 for bubbles situated within the vertical interval $y_b = 0.1 - 0.3$ m. For each of the phase intervals in which the cyclic behavior is discretized, Figure 9 shows the normalized relative horizontal velocity ($U_r(X,Y)$) and the normalized relative vertical velocity ($V_r(X,Y)$), as defined in Equation (21) in the fitting circle $(X,Y)_n^{(F)}$. The experimental results are compared with the potential flow model described in Section 3.1 for $(x/R_b, y/R_b)$ at a radius, R^*, equal to the radius of the fitting circle $(X,Y)_n^{(F)}$. Note that different values of R^* (e.g. ranging between 1.4 and 1.6) among the different vibration phase intervals in which the solids are averaged may promote changes in the velocity of solids predicted by the potential flow theory. As commented previously, the horizontal component of the bubble velocity of each individual bubble is very reduced compared to the vertical component so that $\theta_b \simeq 0$ and Equations (9) and (10) are used. Also, the averaging of different bubbles compensates the inaccuracies arising from considering $\theta_b = 0$.

In Figure 9, the potential flow model provides a very good prediction in terms of the behavior of the solids velocity as a function of the angle, θ, of their position. Nevertheless, in the phase interval $\phi = 0.25\pi - 1.5\pi$ rad (Figure 9(b,f)) the magnitude of the horizontal solids velocity in the experiments is smaller than in the rest of phase intervals. In this phase interval, the particles around the bubble are dragged downward affected by the downward bed bulk motion in the proximity of the bubble, as evidenced in Figures 7 and 8, which reduces the horizontal component of the solids velocity around the bubble.

Besides, a reduction of the magnitude of the vertical velocity of solids is found at $\theta = \pm 90°$ in the phase interval $\phi = 0.25\pi - 0.5\pi$ rad. This behavior was also observed in Figures 7 and 8 and is attributed to the decrease of the solids velocity in the regions close to the bubble. In that phase interval, the bed bulk compression is maximum, which reduces both the solids and the bubble velocity. The reduction of the solids velocity in the regions close to the bubble could be also observed in Figure 7(b,c) for the absolute velocity

15

of solids. Additionally, the largest velocity of the particles in the wake region of the bubble ($\theta \simeq \pm 180°$), when they are affected by the compression wave front of particles caused by bed vessel ascending stroke, is manifested in Figure 9 in a phase range $\phi = 1.75\pi - 0.25\pi$ rad.

To characterize the uncertainty associated to the averaging of bubbles method, the minimum and maximum standard deviation of the normalized relative velocity profiles (Figure 9) for $M = 8$ phase intervals was computed, resulting in values of the standard deviation, σ, between 0.1 and 0.35. This indicates that the uncertainty ($\sigma/N_f^{1/2}$) associated to the mean profiles of normalized velocity around the bubble is between $0.9 \cdot 10^{-2}$ and $3.2 \cdot 10^{-2}$. This uncertainty range can be considered acceptable for the bubble averaging methodology employed. Similar values are obtained for the solids velocity profiles in regions out of the fitting circle.

[Figure 9 about here.]

The results shown in Figures 7 to 9 correspond to bubbles whose centroids were situated at a height interval of $y_b = 0.1 - 0.3$ m from the distributor. However, as stated in previous works [10, 14, 32], the behavior of bubbles changes as they rise in a vibrated bed. Thus, the solids velocity may also vary as a function of the bubble position in the bed. To quantify the dependence of the solids behavior around the bubble with the vertical position of the bubble, Figure 10 shows the standard deviations, σ_U, and σ_V, of the normalized horizontal and vertical solids relative velocities at the fitting circle $(X, Y)_n^{(F)}$ (i.e. the standard deviation with θ of the curves shown in Figure 9). For the sake of comparison, σ_U and σ_V are calculated for two different vertical intervals $y_b = 0.1 - 0.2$ m (lower section of the bed) and $y_b = 0.2 - 0.3$ m (upper section of the bed) and for a fixed value of $R^* = 1.56$, which corresponds to the largest value of R^* encountered for all the phases and height intervals analyzed in Figure 10. Analysis of the results, not included here for brevity, showed that the curves in Figure 9 preserved a sinusoidal shape regardless the averaging is done for bubbles that are in the upper or in the lower section of the bed. Hence, the standard deviation of the curves in Figure 9 is considered a valid method to measure and compare the amplitude of the angular variation of the oscillation of solids velocities around the bubble (i.e. the amplitude is approximately $\sqrt{2}$ times σ). For non-vibrating conditions, the bubble injection system used in the experiment originated bubbles that tended to break, which precludes a correct calculation of the solids velocity around the isolated bubbles.

The results are compared in Figure 10 with the standard deviation of the solids velocity at $(X, Y)_n^{(F)}$ ($R^* = 1.56$), obtained by means of the Davidson and Harrison [22] model. In addition, the relative discrepancy between the experimental results in the interval $y_b = 0.1 - 0.3$ m and the values predicted by the Davidson and Harrison [22] model are included in Table 2.

The relative discrepancy is calculated as:

$$Dr_{\sigma_{U,V}} = \frac{|\sigma_{U,V,exp} - \sigma_{U,V,Davidson}|}{\sigma_{U,V,Davidson}} \tag{22}$$

where $\sigma_{U,V,exp}$ and $\sigma_{U,V,Davidson}$ are, respectively, the standard deviation of the experimental results for U_r or V_r and that of the results of the Davidson & Harrison's potential model shown in Figure 10.

It can be noted in Figure 10(a) that the amplitude of the angular variation of the normalized horizontal solids velocity (proportional to σ_U) is smaller around a bubble situated in the lower section of the bed than when it is situated in the upper section. This could be attributed to the smaller velocity of the bubbles in the lower section of the bed and to the smaller oscillation of the bed bulk in that section, in which the particles move less freely than in the upper section [15]. The more remarkable differences between the lower and the upper sections of the bed are observed in a phase interval $\phi = 0.5\pi - 1.5\pi$ rad, where the propagation of the expansion wave in the bed takes place, which largely affects the horizontal component of the solids velocity around the bubble (see Figure 6). As depicted in Figure 9, for nearly all the phase intervals shown in Figure 10, σ_U in the experiments presents a standard deviation smaller than in the Davidson and Harrison [22] model. Large differences are observed between the experimental results and the Davidson and Harrison [22] model in the phase interval $\phi = 0.25\pi - 1.75\pi$ rad both in Figure 10(a) and in Table 2, which may reflect the significant effect of the bed bulk cyclic oscillation on the normalized horizontal solids velocity around the bubble during the bed bulk expansion.

The normalized vertical solids velocity also varies with the vertical position of the bubble in the bed in Figure 10(b). Here, the standard deviation (i.e. the magnitude) of the normalized vertical solids velocity is maximum in a phase interval $\phi = 1.5\pi - 0.25\pi$ rad (of the next cycle), as the bubble is strongly affected by the compression wave front generated at the bottom of the bed, as shown in Figure 7. The normalized vertical velocity of solids is smaller for $\phi > 0.25\pi$ rad due to the deceleration of the bed vessel and increases again in Figure 10(b) in an interval $\phi = 0.6\pi - 1.3\pi$ rad owing to the expansion of the bed bulk, which increases the vertical velocity of the solids as they move around the bubble, as in Figure 7. The values obtained for σ_V for bubbles located at $y_b = 0.1 - 0.3$ m are slightly underestimated in the phase interval $\phi = 0.3\pi - 1.6\pi$ rad by the Davidson and Harrison [22] model. Differences typically smaller than 15% are found between the experimental results and the Davidson and Harrison [22] model, as shown in Table 2, whereas larger differences appear in the horizontal velocity. These results imply that the Davidson and Harrison [22] model is capable of qualitatively predicting the motion of solids around a bubble rising in a vibrated fluidized bed in a relative system of reference, despite the bed and the bubbles are cyclically oscillating. These differences in U_r probably arise from the interaction of the bed bulk cyclic oscillation with the solids velocity around the bubble. As also evidenced in Figure 9, for the first and last phase intervals in Figure 10(b) ($\phi = 0 - 0.25\pi$ rad and $\phi = 1.75\pi - 2\pi$ rad), the experimental σ_V is around a 30% above the Davidson and Harrison [22] model results. Besides, as in the case of the solids horizontal velocity, the magnitude of the normalized solids velocity is smaller in the lower section of the bed.

[Figure 10 about here.]

[Table 2 about here.]

Despite the phase dependency cyclic variation of the amplitude of the solids motion around a bubble, Figure 9, all the results shown above confirm the qualitative validity of the Davidson and Harrison [22] model for the solids velocity around an isolated bubble rising in a vertically vibrated fluidized bed. This may suggest that, even if the bed is vertically vibrated, the air velocity field around the bubble develops much faster than the solids velocity, leading to a quasi-stationary state in which the potential flow hypothesis is still applicable.

5.2.1. Effect of the vibration amplitude and frequency

Qualitatively similar results to the ones shown in Figures 7, 8 and 9 were obtained in the experiments for all the frequencies and amplitudes of vibration tested (Table 1). However, quantitative differences regarding the magnitude of the particles velocity around an isolated bubble were found. Figure 11 provides a picture of these differences through the calculation of the standard deviation of the vertical and horizontal velocities along the fitting circle $(X, Y)_n^{(F)}$ for the different vibration conditions. In this case, the results are depicted at $R^* = 1.7$, which corresponds to the largest R^* encountered for all the vibration amplitudes, frequencies and phase intervals in Figure 11.

The decrease of the angular amplitude of the normalized horizontal solids velocity in the phase interval $\phi = 0.25\pi - 1.5\pi$ rad observed in Figures 9 and 10 is manifested for the different vibration conditions tested, as shown in Figure 11, excepting for the smallest vibration amplitude. In Figure 11(a), σ_U decreases when reducing the vibration amplitude. This decrease of the standard deviation of the normalized solids velocity is also manifested in the vertical velocity of particles (Figure 11(c)). This suggests that, for low vibration amplitudes, the normalized horizontal velocity of solids around a bubble is not strongly affected by vibration given the fact that the compression wave, which is the main cause of the wake penetration and the solids velocity fluctuation in regions close to the bubble contour, travels in the vertical direction. A decrease of σ_U and σ_V is also observed when decreasing the vibration frequency in Figures 11(b,d). Vibration at low A or f promotes a decrease of the bed bulk oscillation which, in turn, may reduce the effect of vibration on the motion of solids around a bubble.

[Figure 11 about here.]

6. Conclusions

The motion of solids around isolated bubbles in a pseudo-2D fluidized bed subjected to vertical vibration was experimentally studied in the present work by means of DIA and PIV. The bed was filled with Geldart

18

B particles and vibrated at different amplitudes and frequencies. A bubble averaging methodology was used to analyze, for the first time, the average solids behavior around isolated bubbles as a function of the vibration phase.

As observed in previous works, vibration of the bed vessel promotes the appearance of compression and expansion wave fronts in the solids phase. These waves are generated by the interaction of the bed bulk with the distributor and travel upwards in the bed. The PIV results shown in the present contribution revealed that the motion of solids around a bubble in the vibrated bed and, in particular, in the wake region of the bubble, are strongly affected by the cyclic compression and expansion of the bed bulk. The velocity of the compression wave front seems to remain unaffected as the bubble rises in the bed. However, the velocity of the expansion wave increases as the bubble rises in the bed.

The PIV results of the average solids motion around a bubble revealed that, when expressed in coordinates relative to the bubble front velocity, the solids follow the average bubble contour. This motion resembles that of a potential flow around a bubble in a conventional fluidized bed. Besides, direct comparisons of the experimental results with the classical Davidson and Harrison [22] potential flow model confirmed the validity of this simple model to qualitatively describe the solids motion around the bubbles rising in the vibrated fluidized bed studied in this work. Quantitatively, increasing either the vibration amplitude or the vibration frequency increases both the horizontal and vertical normalized velocity of solids around the bubble.

Overall, the results presented in this work can help to understand the complex mutual interaction of the bubbles and the bed bulk in this kind of vibrated systems. This interaction, in turn, affects the shape of the bubbles and the volume of solids that they drag, which are aspects of great relevance in reactors and chemical conversion processes.

Nomenclature

A = bed vibration amplitude (m)

A_b = bubble area (m^2)

$(x, y)^{(C)}$ = bubble centroid coordinates (m)

D_b = bubble diameter (m)

$Dr_{\sigma_{U,V}}$ = relative discrepancy of potential flow (-)

$(X, Y)^{(P)}$ = fitting circle coordinates (-)

$(X, Y)_n^{(P)}$ = new fitting circle coordinates (-)

f = vibration frequency (Hz)

H = bed height (m)

H_0 = static bed height (m)

K = bed thickness (m)

M = number of phase intervals for averaging of cycles (-)

N = total frames along an experiment (-)

N_b = number of bubbles along an experiment (-)

N_{bins} = number of windows for velocity averaging (-)

N_f = number of samples of a phase interval (-)

$(x, y)^{(P)}$ = bubble perimeter coordinates (m)

R = fitting circle radius (-)

R_b = bubble radius (m)

R^* = radius at which the velocity particles at $\theta = 0°$ reaches a maximum positive value (-)

T = period of vibration (s)

t = time (s)

t_o = time instant (s)

U = horizontal velocity (m/s)

U_{mf} = minimum fluidization velocity (m/s)

U_r = normalized horizontal relative velocity of solids (-)

u = horizontal solids velocity (m/s)

V = vertical velocity (m/s)

$V_b(t)$ = instantaneous vertical velocity of a bubble (m/s)

V_{bed} = equivalent vibration velocity of the vessel (m/s)

V_{bub} = bubble velocity (m/s)

V_r = normalized vertical relative velocity of solids (-)

$\vec{V}_r$ = normalized relative solids velocity vector (-)

$\vec{V}_s(X, Y)$ = normalized solids velocity vector (-)

$\vec{v}_s$ = solids velocity vector (m/s)

$v(t)$ = bed vessel instantaneous velocity (m/s)

v = vertical solids velocity (m/s)

W = bed width (m)

X = normalized horizontal coordinate (-)

x = horizontal coordinate (m)

Y = normalized vertical coordinate (-)

y = vertical coordinate (m)

Greek letters

β = bubble contours (-)

Δt = time increment between two images (s)

$\Delta \phi$ = phase interval (rad)

Δx = vertical striper width (m)

$\delta(t)$ = instantaneous vibration vertical displacement (m)

θ = angle from the vertical direction (°)

θ_b = bubble rising angle (°)

ρ = density (kg/m^3)

σ = standard deviation (-)

Φ = velocity potential (m^2/s)

ϕ = bed vessel vibration phase (rad)

Subscripts

avg = average

b = bubble

bed = bed vessel

c = compression

e = expansion

f = wave front

$prop$ = propagation

r = relative

s = stripe

Acknowledgments

References

[1] Y. Mawatari, Y. Tatemoto, K. Noda, Prediction of minimum fluidization velocity for vibrated fluidized bed, Powder Technol. 131 (2003) 66–70.

[2] Y. Mawatari, M. Tsunekawa, Y. Tatemoto, K. Noda, Favorable vibrated fluidization conditions for cohesive fine particles, Powder Technol. 154 (2005) 54–60.

[3] X. Yang, Y. Zhao, Z. Luo, S. Song, C. Duan, L. Dong, Fine coal dry cleaning using a vibrated gas-fluidized bed, Fuel Process. Technol. 106 (2013) 338–343.

[4] K. Noda, Y. Mawatari, S. Uchida, Flow patterns of fine particles in a vibrated fluidized bed under atmospheric or reduce pressure, Powder Technol. 99 (1998) 11–14.

[5] T. Zhou, H. Kage, S. Funaoka, H. Ogura, Y. Matsuno, Fluidization behaviour of glass beads under different vibration modules, Adv. Powder Technol. 12 (2001) 559–575.

[6] E. Eccles, A. Mujumdar, Bubble phenomena in aerated vibrated beds of small particles, Drying Technol. 15:1 (1997) 95–116.

[7] Y. Mawatari, K. Tagawa, Y. Tatemoto, K. Noda, Bubbling characteristics under vertical vibration in a two-dimensional fluidized bed, Chem. Eng. Jpn. 38 (2005) 18–23.

[8] T. Zhou, H. Ogura, M. Yamamura, H. Kage, Bubble motion pattern and rise velocity in two-dimensional horizontal and vertical vibro-fluidized beds, Can. J. Chem. Eng. 82 (2004) 236–242.

[9] T. Zhou, H. Kage, H. Li, Bubble characteristics in a two-dimensional vertically vibro-fluidized bed, China Partic. 3 (2005) 224–228.

[10] E. Cano-Pleite, Y. Shimizu, A. Acosta-Iborra, Y. Mawatari, Effect of vertical vibration and particle size on the solids hold-up and mean bubble behavior in a pseudo-2D fluidized bed, Chem. Eng. J. 304 (2016) 384–398.

[11] J. Laverman, H. Roghair, M. van Sint Annaland, H. Kuipers, Investigation into the hydrodynamics of gas-solid fluidized beds using particle image velocimetry coupled with digital image analysis, Can. J. Chem. Eng. 86 (2008) 523–535.

[12] F. Hernández-Jiménez, S. Sánchez-Delgado, A. Gómez-García, A. Acosta-Iborra, Comparison between two-fluid model simulations and particle image analysis & velocimetry (PIV) results for a two-dimensional gas-solid fluidized bed, Chem. Eng. Sci. 66 (2011) 3753–3772.

[13] A. Busciglio, G. Vella, G. Micale, L. Rizzuti, Analysis of the bubbling behaviour of 2D gas solid fluidized beds: Part I. digital image analysis technique, Chem. Eng. J. 140 (2008) 398–413.

[14] E. Cano-Pleite, F. Hernández-Jiménez, A. Acosta-Iborra, Y. Mawatari, Oscillatory behavior of the bed bulk and the bubbles in a vertically vibrated pseudo-2D bed in bubbling regime, Chem. Eng. J. 312 (2017) 228–242.

[15] E. Cano-Pleite, F. Hernández-Jiménez, A. Acosta-Iborra, Bulk oscillation and velocity wave propagation in a vibrated fluidized bed at minimum fluidization conditions, Powder Technol. 308 (2017) 346–361.

[16] E. Cano-Pleite, F. Hernández-Jiménez, A. Acosta-Iborra, T. Tsuji, C. Müller, Segregation of equal-sized particles of different densities in a vertically vibrated fluidized bed, Powder Technol. 316 (2017) 101–110.

[17] D. Barletta, P. Russo, M. Poletto, Dynamic response of a vibrated fluidized bed of fine and cohesive powders, Powder Technol. 237 (2013) 276–285.

[18] C. Müller, J. Davidson, J. Dennis, A. Hayhurst, A study of the motion and eruption of a bubble at the surface of a two-dimensional fluidized bed using particle image velocimetry (PIV), Ind. Eng. Chem. Res. 46 (2007) 1642–1652.

[19] J. Almendros-Ibáñez, C. Sobrino, M. de Vega, D. Santana, A new model for ejected particle velocity from erupting bubbles in 2-d fluidized beds, Chem. Eng. Sci. 61 (2006) 5981–5990.

[20] D. Santana, S. Nauri, A. Acosta, N. Garcia, A. Macias-Machín, Initial particle velocity spatial distribution from 2-d erupting bubbles in fluidized bed, Powder Technol. 150 (2005) 1–8.

[21] S. Sánchez-Delgado, C. Marugán-Cruz, A. Acosta-Iborra, D. Santana, Dense-phase velocity fluctuation in a 2-d fluidized bed, Powder Technol. 200 (2010) 37–45.

[22] J. Davidson, D. Harrison, Fluidised Particles, Cambridge University Press, Cambridge, 1963.

[23] F. Hernández-Jiménez, J. Third, A. Acosta-Iborra, C. Müller, Comparison of bubble eruption models with two-fluid simulations in a 2D gas-fluidized bed, Chem. Eng. J. 171 (2011) 328–339.

[24] C. Zeilstra, M. van der Hoef, J. Kuipers, Experimental and numerical study of solids circulation in gas-vibro fluidized beds, Powder Technol. 248 (2013) 153–160.

[25] E. Cano-Pleite, F. Hernández-Jiménez, A. Acosta-Iborra, C. Müller, Reversal of gulf stream circulation in a vertically

vibrated triangular fluidized bed, Powder Technol. 316 (2017) 345–356.

[26] L. Xiang, W. Shuyan, L. Huilin, L. Goudong, C. Juhui, L. Yikun, Numerical simulation of particle motion in vibrated fluidized beds, Powder Technol. 197 (2010) 25–35.

[27] Y. Tatemoto, Y. Mawatari, T. Yasukawa, K. Noda, Numerical simulation of particle motion in vibrated fluidized bed, Chem. Eng. Sci. 59 (2004) 437–447.

[28] D. Barletta, M. Poletto, Aggregation phenomena in fluidization of cohesive powders assisted by mechanical vibrations, Powder Technol. 225 (2012) 93–100.

[29] J. Sun, F. Battaglia, S. Subramaniam, Dynamics and structures of segregation in a dense, vibrating granular bed, Phys. Rev. E. 74 (2006) 1–13.

[30] L. Sun, F. Zhao, Q. Zhang, D. Li, H. Lu, Numerical simulation of particle segregation in vibration fluidized bed, Chem. Eng. Technol. 37(12) (2014) 2109–2115.

[31] P. Zhao, Y. Zhao, Z. Chen, Z. Luo, Dry cleaning of fine lignite in a vibrated gas-fluidized bed: Segregation characteristics, Fuel 142 (2015) 274–282.

[32] E. Cano-Pleite, F. Hernández-Jiménez, M. de Vega, A. Acosta-Iborra, Experimental study on the motion of isolated bubbles in a vertically vibrated fluidized bed, Chem. Eng. J. 255 (2014) 114–125.

[33] E. Cano-Pleite, F. Hernández-Jiménez, A. Acosta-Iborra, Compressible-gas two-fluid modeling of isolated bubbles in a vertically vibrated fluidized bed and comparison with experiments, Chem. Eng. J. 271 (2015) 287–299.

[34] D. Geldart, Types of gas fluidization, Powder Technol. 7 (1973) 285.

[35] E. Cano-Pleite, Fundamental studies on vibrated fluidized beds, PhD. Thesis, Carlos III University of Madrid (2016).

[36] N. Otsu, A threshold selection method from gray-level histograms, IEEE Trans. Syst. Man. Cybern. 9 (1979) 62–66.

[37] J. Sveen, Matpiv, in: https://www.mn.uio.no/math/english/people/ aca/jks/matpiv/.

[38] R. Keanke, R. Adrian, Theory of cross-correlation analysis of PIV images, Comput. Graphics Image Process. 49 (1992) 191–215.

[39] R. Roy, J. Davidson, V. Tuponogov, The velocity of sound in fluidised beds, Chem. Eng. Sci. 45 (1990) 3233–3245.
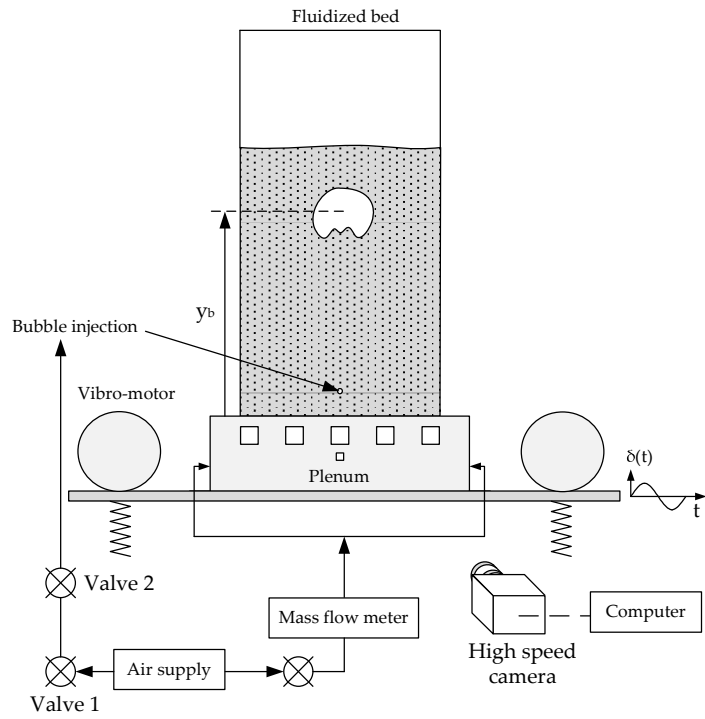
List of Figures

24

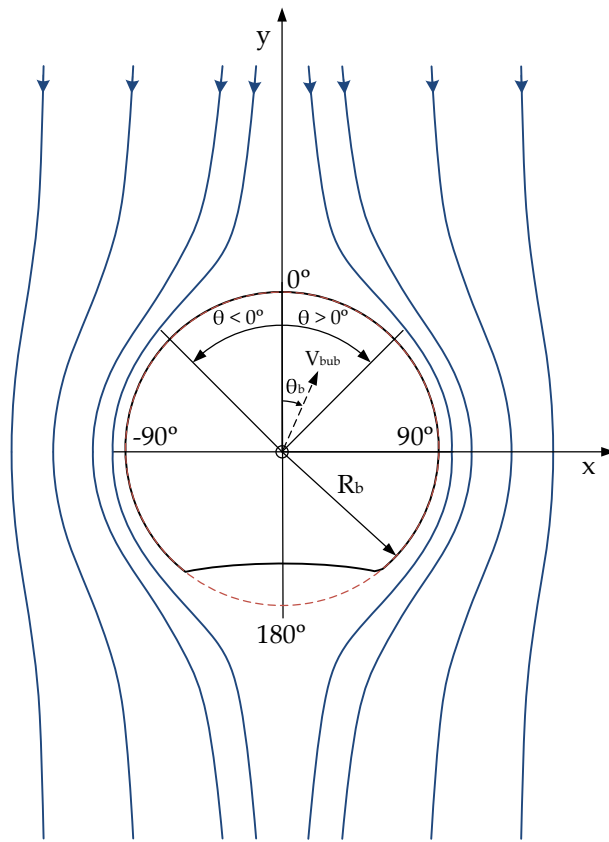Figure 1: Sketch of the experimental facility.

Figure 2: Schematic drawing of the potential flow theory of Davidson and Harrison [22] showing the theoretical particle tracks.
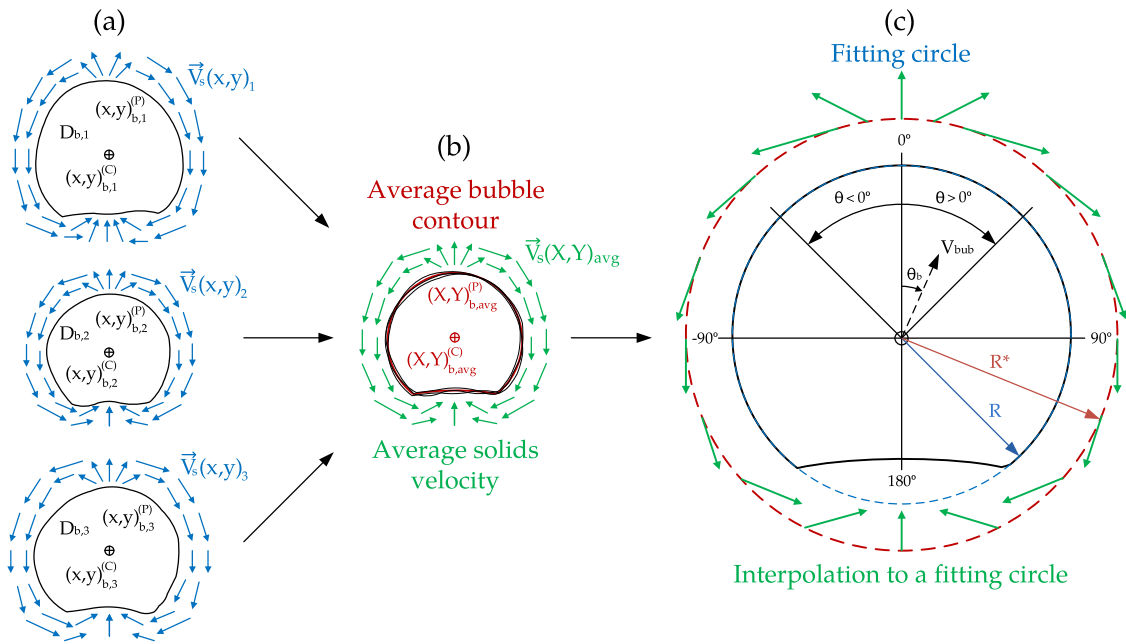
Figure 3: Sketch of the bubbling averaging method. The left hand side of the figure shows the sampling of multiple bubbles and solids velocities to produce the average bubble contour and the average distribution of solids velocity. The right hand side of the figure sketches the fitting circle and the definition of the angle θ.
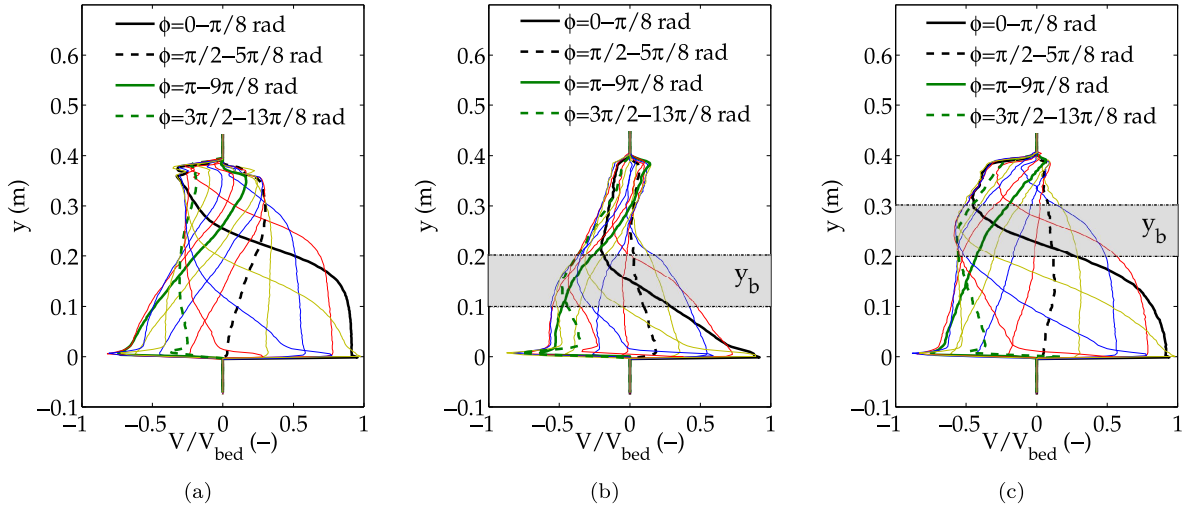
Figure 4: Vertical evolution of the normalized absolute vertical velocity of the solids in the bed for different phase intervals: (a) No bubble present in the system, (b) bubble in the height interval $y_b = 0.1 - 0.2$ m, and (c) bubble in the height interval $y_b = 0.2 - 0.3$ m. The red, blue and yellow lines represent intermediate phase intervals of $\Delta\phi = \pi/8$ rad placed between the phase intervals defined in the legend of the figures. The horizontal black line indicates the average position of the bubble in each figure. Exp. 1.
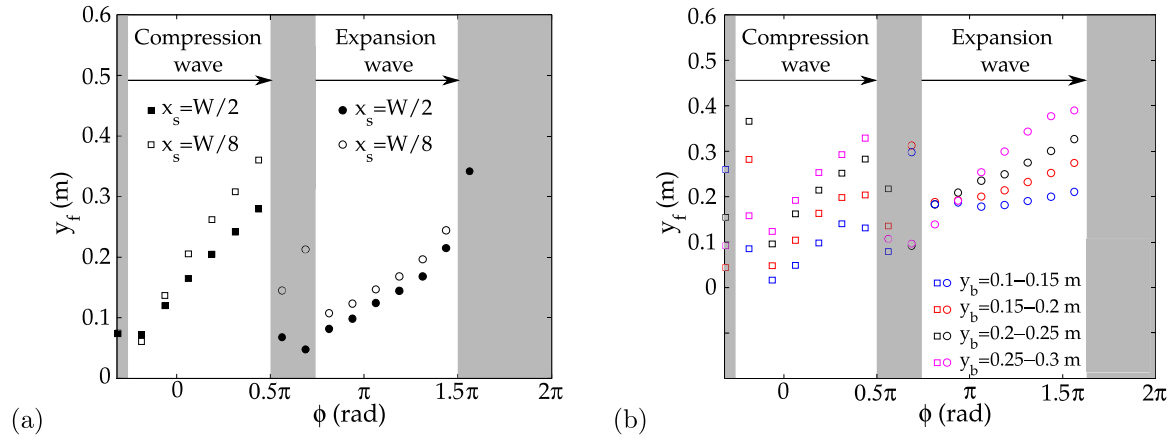
Figure 5: Vertical positions of the compression and expansion wave fronts as a function of the vibration phase. (a) No bubble in the bed and (b) Bubble rising within different height intervals. Exp. 1.
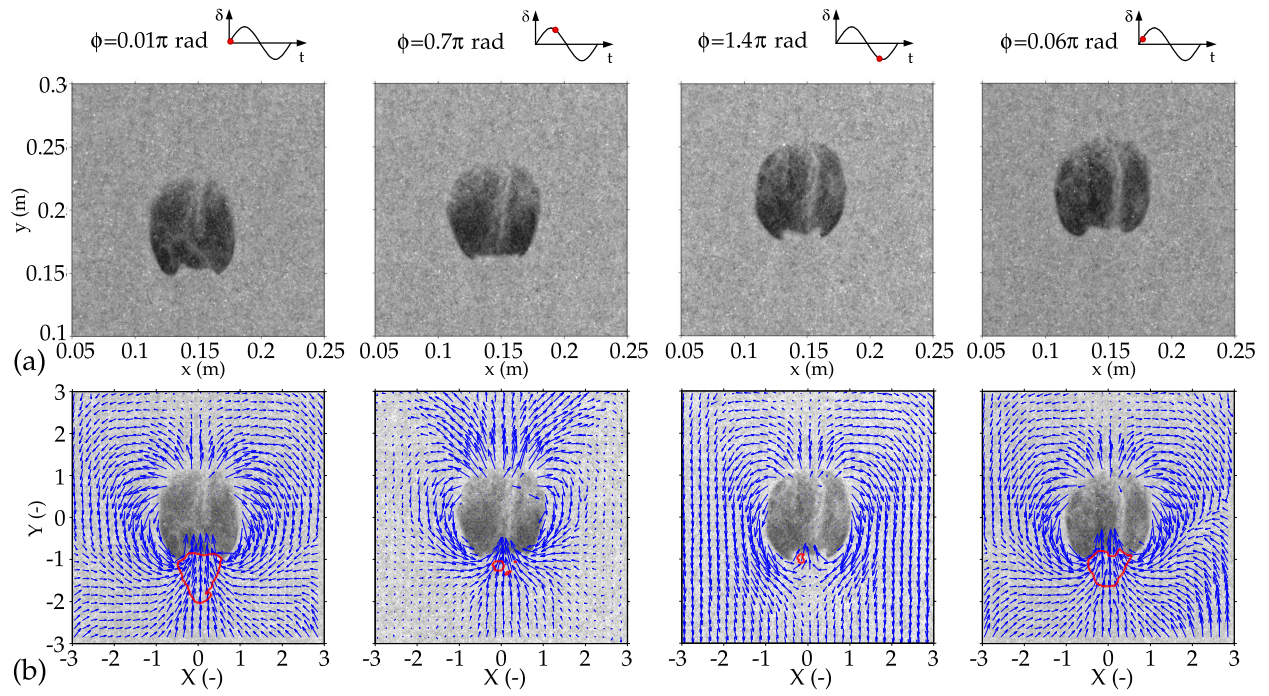
Figure 6: Grayscale digital images of an isolated bubble rising in the vibrated fluidized bed and captured at different vibration phases. (a) Original images in an absolute system of coordinates. (b) Instantaneous absolute solids velocity superimposed to the captured images in the normalized coordinate system (X, Y). The red lines delimit the regions belonging to the bubble wake volume. Exp. 1.
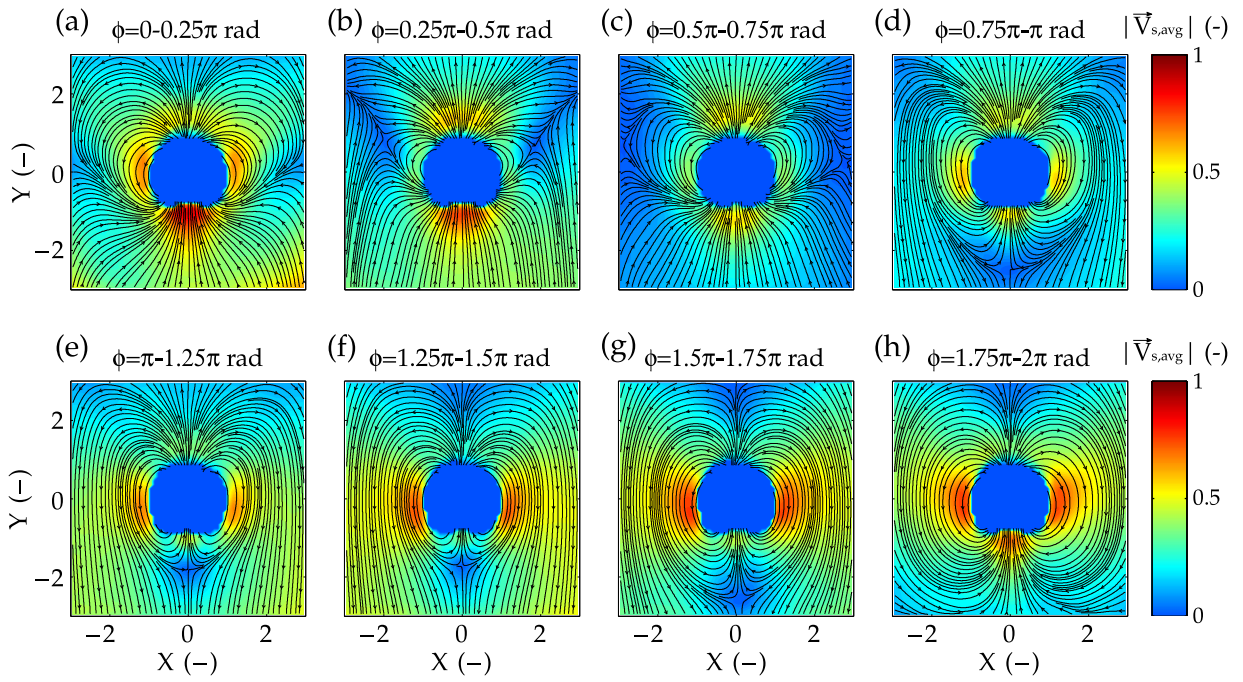
Figure 7: Streamlines of the normalized absolute solids velocity around the equivalent bubble contour resulting from the bubble averaging method in the vertically vibrated fluidized bed. Results are presented for eight different phase intervals of size $\Delta\phi = 0.25\pi$ rad over a total interval of $\phi = 0 - 2\pi$ rad. The solid streamlines are shown superimposed to the velocity magnitude maps. Exp. 1.
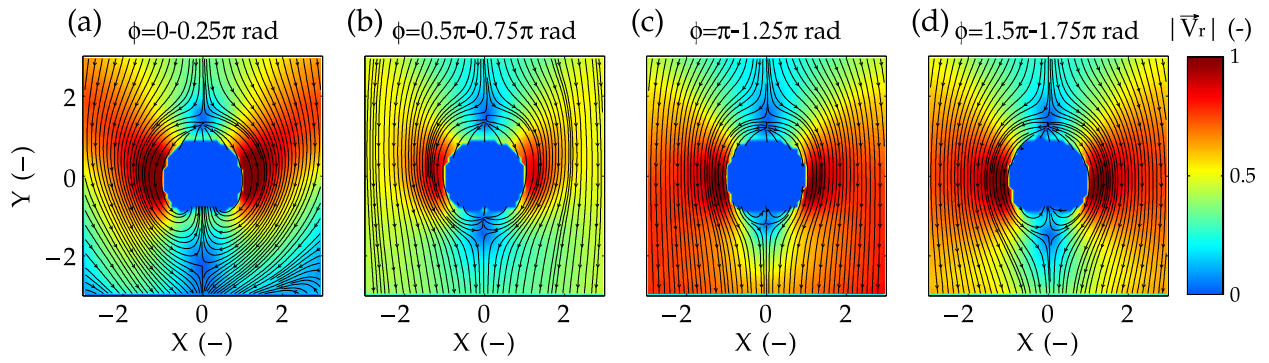
Figure 8: Streamlines of the normalized relative solids velocity around the equivalent bubble contour resulting from the bubble averaging method in the vertically vibrated fluidized bed. Results are presented for four different phase intervals of size $\Delta\phi = 0.25\pi$ rad over a total interval of $\phi = 0 - 2\pi$ rad. The solid streamlines are shown superimposed to the velocity magnitude maps. Exp. 1.
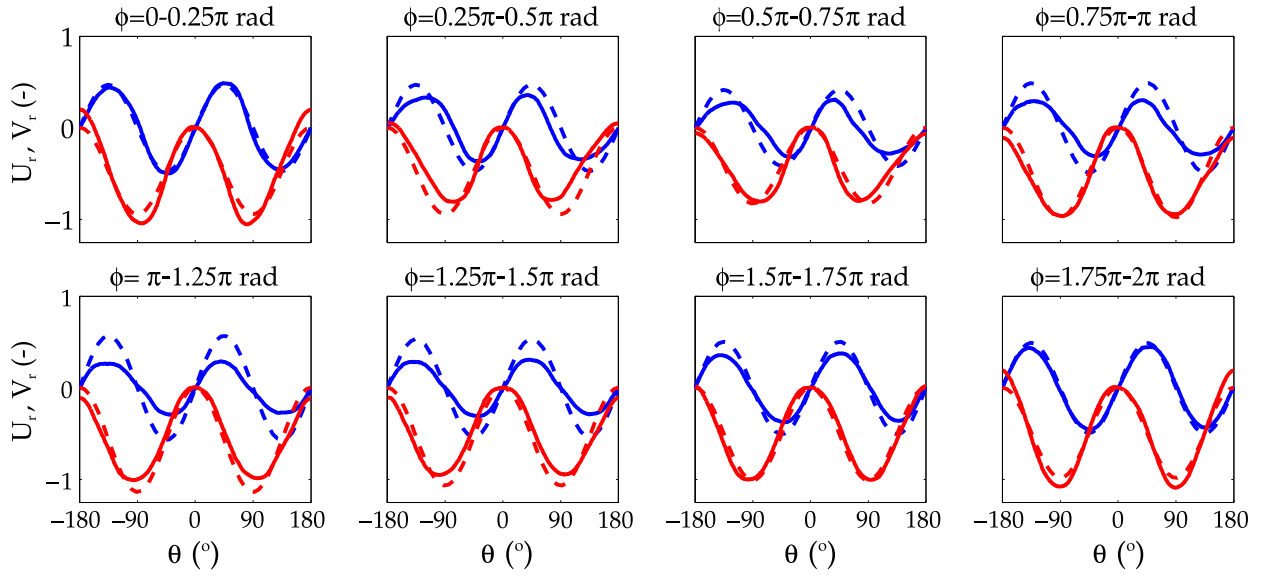
Figure 9: Normalized relative solids velocity at the fitting circle of the bubble contour for eight different phase intervals of size $\Delta\phi = 0.25\pi$ rad over a total interval $\phi = 0 - 2\pi$ rad. The blue and red lines correspond, respectively, to the horizontal and vertical solids relative velocities and the dashed lines to the potential flow theory. Exp. 1.
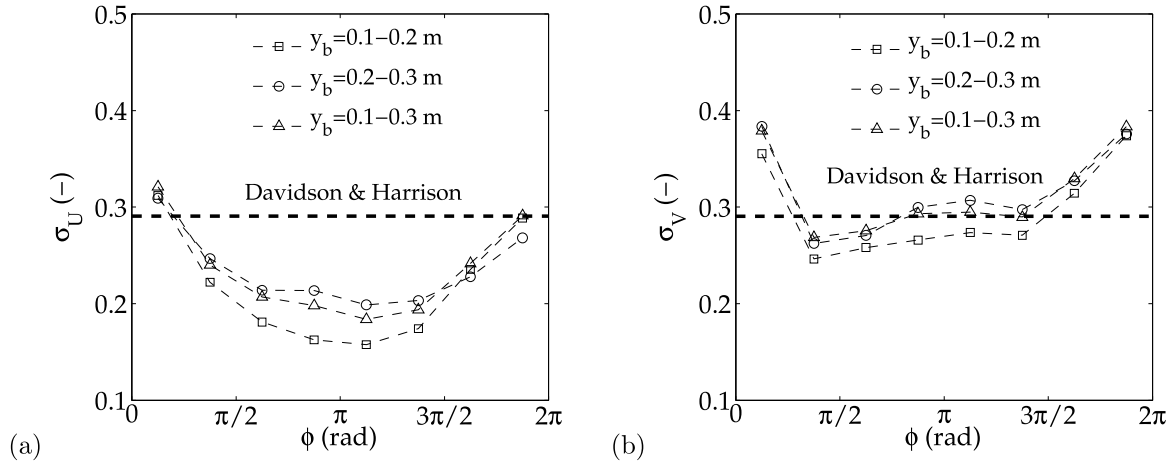
Figure 10: Standard deviation of the normalized solids velocity at the fitting circle ($R^* = 1.56$) for eight different phase intervals of size $\Delta\phi = 0.25\pi$ rad and for bubbles situated in the upper and lower sections of the bed: (a) horizontal component and (b) vertical component of the solids velocity. The horizontal dash line indicates the standard deviation predicted by Davidson and Harrison [22] for bubbles situated at $y_b = 0.1 - 0.3$ m. Exp. 1.
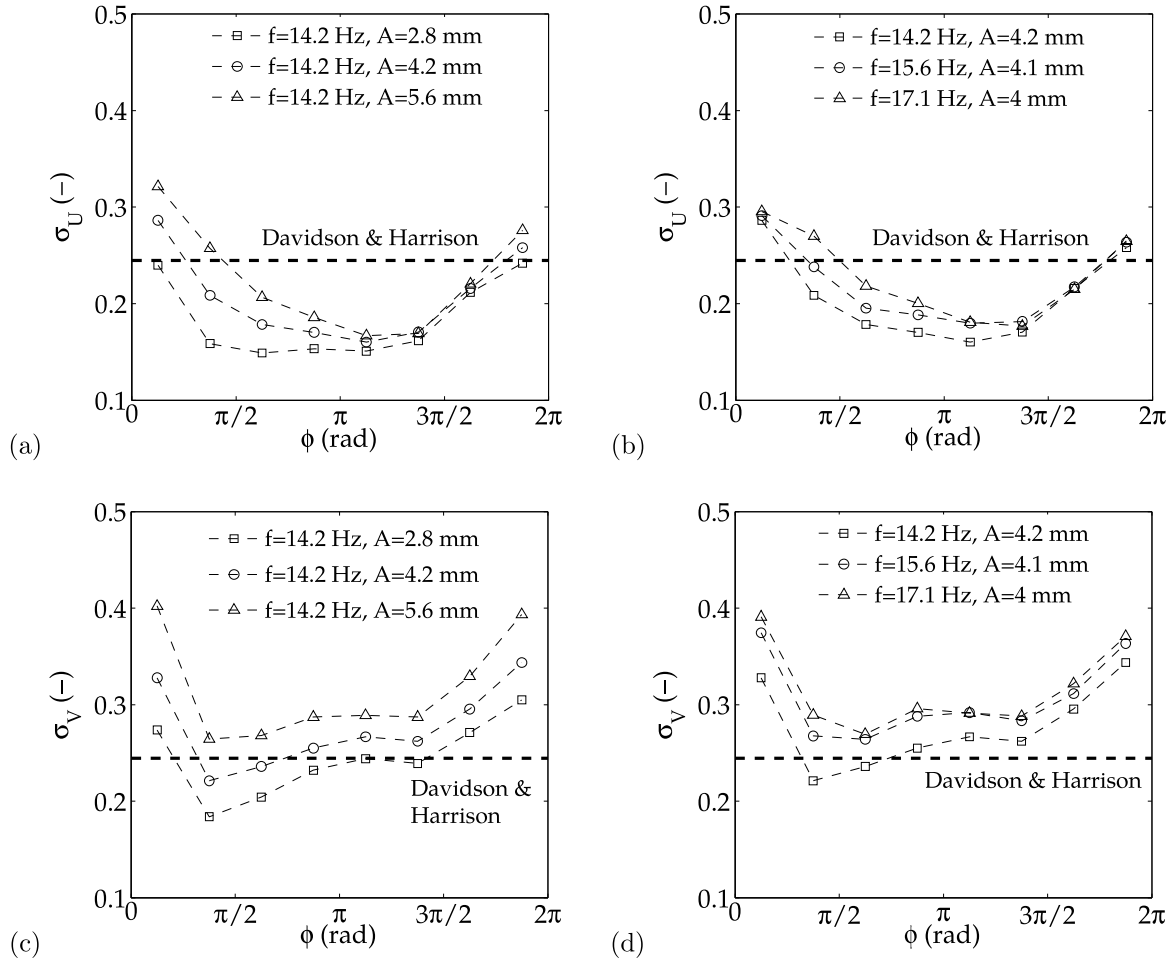
Figure 11: Standard deviation of the (a,b) horizontal and (c,d) vertical normalized solids velocity at the fitting circle ($R^* = 1.7$) for eight different phase intervals of size $\Delta\phi = 0.25\pi$ rad and for bubbles situated in the upper and lower sections of the bed. (a,c) Variation of the vibration amplitude (Exp. 1, 2 and 3) (b,d) Variation of the vibration frequency (Exp. 1, 4 and 5).

List of Tables

Table 1: Experimental conditions.

Exp.	Vibration frequency f (Hz)	Vibration amplitude A (mm)
1	14.2	4.2
2	14.2	2.8
3	14.2	5.6
4	15.6	4.1
5	17.1	4

Table 2: Relative discrepancy of the standard deviation of the normalized solids velocity found between the experimental results and the Davidson and Harrison [22] model at $R^* = 1.56$. Exp. 1, $y_b = 0.1 - 0.3$ m.

ϕ (rad)	Dr_{σ_U} (-)	Dr_{σ_V} (-)
$0 - 0.25\pi$	0.1	0.3
$0.25\pi - 0.5\pi$	0.17	0.08
$0.5\pi - 0.75\pi$	0.29	0.05
$0.75\pi - \pi$	0.32	0.01
$\pi - 1.25\pi$	0.37	0.01
$1.25\pi - 1.5\pi$	0.33	0.004
$1.5\pi - 1.75\pi$	0.17	0.13
$1.75\pi - 2\pi$	0.002	0.32